RENORMALIZATION-GROUP THEORY OF CLASSICAL AND QUANTUM SYSTEMS WITH FROZEN DISORDER

by

Cihan Nadir Kaplan

A Thesis Submitted to the
Graduate School of Sciences
in Partial Fulfillment of the Requirements for
the Degree of

Master of Science

in

Physics

Koç University

August, 2008

Koç University

Graduate School of Sciences and Engineering

This is to certify that I have examined this copy of a master's thesis by

Cihan Nadir Kaplan

and have found that it is complete and satisfactory in all respects,
and that any and all revisions required by the final
examining committee have been made.

Committee Members:

Prof. A. Nihat Berker

Assoc. Prof. F. Gülay Acar

Assist. Prof. Alkan Kabakçıoğlu

Date: _____

To my grandfather

ABSTRACT

In the first part of this thesis, the spin-1/2 quantum Heisenberg spin-glass system is studied in all spatial dimensions d by renormalization-group theory. Strongly asymmetric phase diagrams in temperature and antiferromagnetic bond probability p are obtained in dimensions $d \geq 3$. The asymmetry at high temperatures approaching the pure ferromagnetic and antiferromagnetic systems disappears as d is increased. However, the asymmetry at low but finite temperatures remains in all dimensions, with the antiferromagnetic phase receding from the ferromagnetic phase. A finite-temperature second-order phase boundary directly between the ferromagnetic and antiferromagnetic phases occurs in $d \geq 6$, resulting in a new multicritical point at its meeting with the boundaries to the paramagnetic phase. In $d = 3, 4, 5$, a paramagnetic phase reaching zero temperature intervenes asymmetrically between the ferromagnetic and reentrant antiferromagnetic phases. There is no spin-glass phase in any dimension [1].

In the second part, we focus on the thermodynamic properties of Apollonian networks (AN) using renormalization-group theory. Our calculations, for (1) ferromagnetic (F) percolation models and both (2) antiferromagnetic (AF) and (3) weakened-AF percolation models, reveal no finite-temperature phase transition for the entire range of bond probability p, exhibiting an infinite F phase for (1) and an infinite SG-like phase for (2) and (3). However, the Ising spin glass studied on an AN small-world network shows a phase transition as p is increased, between the F and SG-like phases, as a function of disorder, for all temperatures T. We develop an exact recursion matrix method to calculate nonuniform local order parameters. The calculation of the average magnetization and the SG order parameter shows that the phase boundary between F and SG-like phases is first order, governed by a nonuniform fixed distribution. The exact values of the local order parameters, as functions of the interactions, show complicated distributions. Analysis of the parameters reveals correlations of the F phase within the SG-like phase [2].

ÖZETÇE

Tezin ilk kısmında, spin-1/2 kuantum Heisenberg spin camı modeli her d boyut için, renormalizasyon grubu kuramı kullanılarak hesaplanmıştır. Sıcaklık ve antiferromanyetik bağ yoğunluğu p'ye bağlı olarak, $d \geq 3$ için güçlü asimetrik faz diyagramlar elde edilmiştir. d'nin artmasıyla, saf ferromanyetik ve antiferromanyetik sistemlere yaklaşıldıkça, yüksek sıcaklıklardaki asimetri kaybolmaktadır. Öte yandan düşük ve orta sıcaklıklarda, antiferromanyetik fazın ferromanyetik fazdan çekinmesi şeklindeki asimetri her d boyutta mevcuttur. $d \geq 6$'da, ferromanyetik ve antiferromanyetik fazlar arasında, paramanyetik fazla buluştuğu noktada yeni bir çoklu kritik noktaya yol açan, ikinci dereceden direk bir faz geçişi bulunmaktadır. $d = 3, 4, 5$'te sıfır sıcaklığa kadar uzanan paramanyetik faz, ferromanyetik ve antiferromanyetik fazı asimetrik biçimde ayırmaktadır. Hiçbir boyutta spin camı (SC) fazı gözlenmemiştir.

İkinci kısımda, renormalizasyon grubu kuramı kullanılarak Apollon küçük dünya ağlarının termodinamik özellikleri incelenmiştir. (1) Ferromanyetik (F) perkolasyon ve hem (2) antiferromanyetik (AF), hem de (3) zayıflatılmış antiferromanyetik perkolasyon modelleri için yapılan hesaplarda, hiçbir bağ olasılığı p için sonlu sıcaklıkta faz geçişi gözlenmemiş, (1) için sonsuz bir F faz, (2) ve (3) için sonsuz bir SC benzeri faz elde edilmiştir. Öte yandan, Apollon küçük dünya ağında Ising spin camı modelinde, bağ yoğunluğu p artırıldıkça, F ve SC benzeri fazlar arasında tüm sıcaklıklarda faz geçişi bulunmaktadır. Sistemin düzen parametrelerinin kesin çözümü için bir tekrarlama matrisi yöntemi geliştirilmiştir. Hesaplanan ortalama mıknatıslanma ve SC düzen parametreleri, F ve SC benzeri fazlar arasındaki faz geçişinin birinci dereceden olduğunu ve sabit bir bağ dağılımı tarafından yönetildiğini ortaya koymuştur. Bağ dağılımının fonksiyonu olan düzen parametrelerinin kesin çözümleri, komplike dağılımlar göstermektedir. İncelenen düzen parametreleri, SC benzeri fazın içinde F korelasyonlar olduğuna işaret etmektedir.

ACKNOWLEDGMENTS

I thank everyone whom I am going to miss when I go to the U.S. for my doctoral studies. This includes my family – I think now they are happy seeing me becoming an autonomous person – my close relatives, my roommates and all my friends, and also my advisor Nihat Berker, who made a great contribution to me as a person and as a physicist, my collaborator Michael Hinczewski because of his great enthusiasm and willingness to work, and finally my former and present officemates whom I hope to see frequently in the U.S. From now on, I will be on my own, away from Turkey, so I acknowledge everyone who, in the future, will contribute to the happiness of my life in the U.S. and close connections between me and my home country.

TABLE OF CONTENTS

LIST OF TABLES

LIST OF FIGURES

NOMENCLATURE

RG	renormalization group
AF	antiferromagnetic
F	ferromagnetic
SG	spin glass
P	paramagnetic
nn	nearest neighbor
AN	Apollonian network
DAN	deterministic Apollonian network
RAN	random Apollonian network
EAN	evolutionary Apollonian network

Chapter 1

INTRODUCTION

1.1 Phase Transitions

The equation of state of a thermodynamic system, $f(\vec{K}) = 0$, where each element of $\vec{K}$ is a macroscopic parameter of the system (such as pressure P, volume V, temperature T, for a fluid system), defines a surface in an N-dimensional space, where N is the dimension of $\vec{K}$. In thermodynamic equilibrium, each of the regions in the N-dimensional parameter space which differs from other regions by the behaviour of its thermodynamic potentials, densities and response functions is called a phase. Changing the macroscopic parameters so that the system enters a new phase is called a phase transition.

According to Ehrenfest's and Fisher's classifications, a first-order phase transition occurs where the free energy is singular, and the first derivative of the free energy with respect to one or more of the macroscopic parameters is discontinuous, whereas a discontinuity or divergence in the second derivative of the free energy is defined as a second-order phase transition [3].

1.1.1 First-Order Phase Transitions

At temperature $T = 0$, a transition may occur from the ground state of a phase to the ground state of another phase. At a finite temperature T, there may be a transition between states which are perturbations of the ground states of different phases. When this transition is abrupt, then these two states coexist on the phase transition line which results in discontinuities in the first derivatives of the free energy. Such phase transitions are defined as first-order phase transitions.

As an example, the phase diagrams of fluid and magnetic systems are shown in Figures 1.1 and 1.2. The PT projection of the $P\rho T$ parameter space of a fluid system, where ρ

is the density, exhibits three phases, namely solid, liquid and gaseous phases separated by first-order transition lines except for the critical point denoted by C which terminates the first-order phase boundary between liquid and gas phases. The ρT projection indicates that there is a jump between the densities of liquid and gaseous states which coexist on the first-order transition line. Similarly, the HT projection of the HMT parameter space of a uniaxial magnetic system, where H is external magnetic field and M is magnetization, and H-field is oriented along the axis of magnetization, includes ferromagnetic and paramagnetic phases. On the first-order phase boundary the two ferromagnetic phases, where most of the spins are aligned either in one direction or its opposite, coexist. At temperatures $T > T_c$ there is a paramagnetic phase, where the magnetization is zero for $H = 0$.

For the magnetic system, the order parameter, which is chosen such that it is finite in first-order transitions and vanishes in second-order phase transitions, is given by

$$M \equiv \langle s_i \rangle = \frac{1}{N} \frac{\partial}{\partial H} \log Z \,, \tag{1.1}$$

where s_i is the spin component along the H-field direction, and N is the number of spins. In Fig. 1.2 (b), there is the appearance of non-zero magnetization at zero magnetic field for $T < T_c$, with the sign of magnetization either positive or negative. This phenomenon, called spontaneous symmetry breaking, results in a discontinuity in the first derivative of the free energy with respect to H at $H = 0$. For a fluid system, the order parameter of the lquid-gas transition is given by the density difference between the liquid and gas phases, $\rho_l - \rho_g$, since it is finite for $T < T_c$ and vanishes for $T \geq T_c$, as shown in Fig. 1.1 (b).

It is in fact straightforward to show that the HMT parameter space is analogous to the $P\rho T$ parameter space, as will be discussed in Section 1.1.4.

1.1.2 Second-Order Phase Transitions

In Figs. 1.1 and 1.2 at $T = T_c$ there is no discontinuity in the order parameters, and this type of phase transition is called a second-order phase transition. However, if one looks at the thermodynamic response functions such as the specific heat C_v for the fluid system or the isothermal susceptibility χ_T for the magnetic system, one expects a singularity or a divergence in these functions which arises from the behavior of the order parameters as a function of T at the critical point. Since the thermodynamic response functions are the

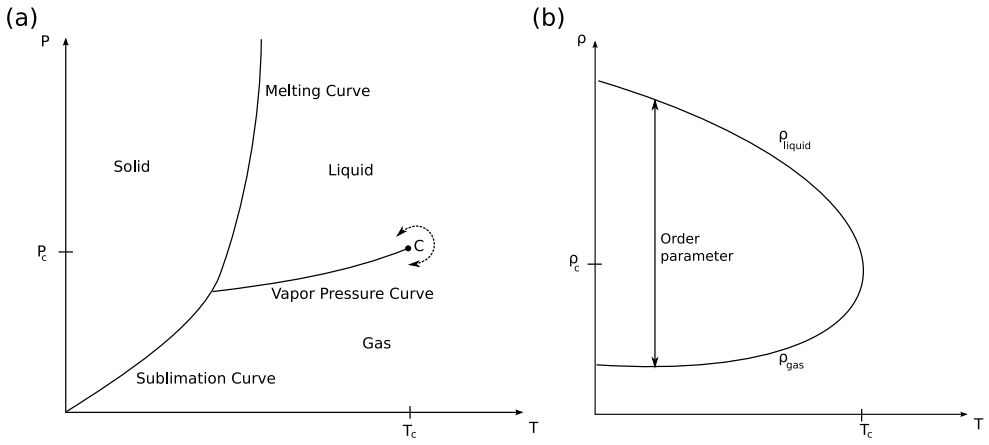

Figure 1.1: Phase diagrams of a fluid [4]. Note that the phase boundary between solid and liquid phases does not terminate in a critical point because of the absence of translational symmetry in the solid phase.

second derivatives of the free energy, a singularity or divergence in these type of functions was classified by Fisher and Ehrenfest as a second-order phase transition [3].

Consider the behavior o a thermodynamic quantity Q, a first derivative of the free energy, as the macroscopic parameter K_α is varied, with all other parameters $K_{\beta\neq\alpha}$ fixed. Then, the thermodynamic response function R is given by

$$R \sim \left[\frac{\partial Q}{\partial K_\alpha}\right]_{K_{\beta\neq\alpha}} . \tag{1.2}$$

For instance, the specific heat for a magnetic system is of the form

$$C_H = \left[\frac{\partial U}{\partial T}\right]_H , \tag{1.3}$$

where U is the internal energy. The specific heat either diverges or stays finite, exhibiting a cusp. In the latter case, the derivative of the specific heat is discontinuous, and the phase transition is again classified as second order.

Large fluctuations at all length scales are observed in a system at its critical point, since the correlation length ξ goes to infinity. That is, in a magnetic system, there are islands of infinite size[1] which have positive, negative or zero magnetizations fluctuating at all length scales, showing a fractal behavior [5]. Hence, the system is said to be scale invariant, as will be discussed in more detail in the next section.

[1]The term infinite size refers to a system in its thermodynamic limit, namely the number of microscopic components of the system are in the order of $\sim 10^{23}$.

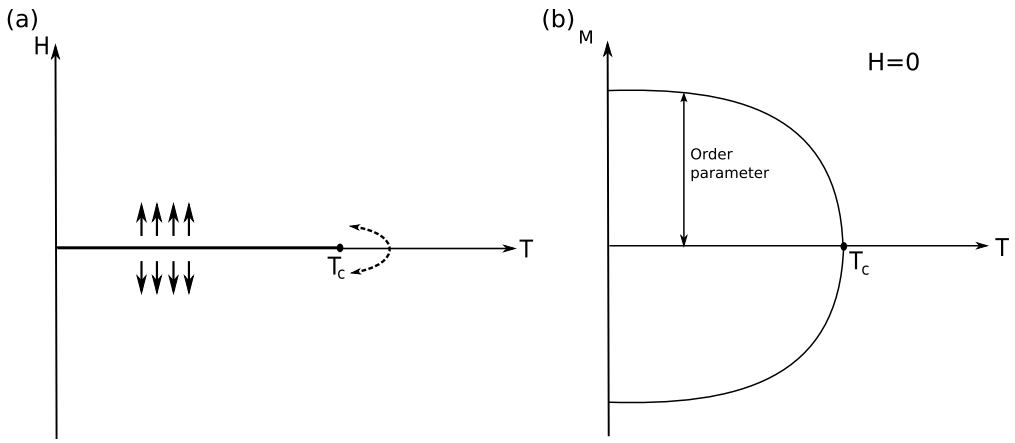

Figure 1.2: Phase diagrams of a magnetic system [4].

1.1.3 Scale Invariance

As mentioned in section 1.1.2, at a critical point, there are fluctuations at all length scales, leading to scale invariance, or in other words, self similarity. The fractal structure results from the competition of fluctuating long-range and short-range orders. That is, one will always see the same structure regardless of the scale at which one looks at the system. Mathematically, a critical point, where the self-similarity occurs, is a singular point, where the entire set of thermodynamic functions exhibit power-law singularities. Thus, it is appropriate to assign an exponent λ to each function $F(t)$ [4]:

$$\lambda = \lim_{t \to 0} \frac{\log |F(t)|}{\log |t|}, \quad \text{where} \quad t \equiv \frac{T - T_c}{T_c}. \tag{1.4}$$

That is,

$$F(t) \sim |t|^{\lambda}. \tag{1.5}$$

Each of the critical exponents for the thermodynamic functions is marked with a Greek letter. Table 1.1 indicates some critical exponents for fluid and magnetic systems.

1.1.4 Universality

The microscopic details of the system are usually irrelevant near the second-order phase transitions [5], leading to a principle called universality: systems with different microscopic components may behave similarly near the critical point.

	Fluid System	Magnetic System
Specific Heat	$C_V \sim \|t\|^{-\alpha}$	$C_H \sim \|t\|^{-\alpha}$
Order Parameter	$\rho_l - \rho_g \sim (-t)^{\beta}$	$M \sim (-t)^{\beta}$
Isothermal Response Function	$\kappa_T \sim \|t\|^{-\gamma}$ (Compressibility)	$\chi_T \sim \|t\|^{-\gamma}$ (Susceptibility)
Critical Isotherm($t = 0$)	$P - P_c \sim \|\rho_l - \rho_g\|^{\delta}$	$H \sim \|M\|^{\delta}$
Correlation Length	$\xi \sim \|t\|^{-\nu}$	$\xi \sim \|t\|^{-\nu}$

Table 1.1: Definitions of some critical exponents for fluid and magnetic systems [4].

The equivalence between fluid and magnetic systems is quite straightforward. A two-state magnetic system which consists of classical interacting up and down spins is described by the Ising model. On the other hand, a fluid system can be mapped to a lattice-gas model as follows [3]: The volume V of the fluid system is divided into fixed volumes v. In every v, there is either a molecule or v is empty. Then the interactions between the molecules can be thought of as interactions between the fixed volumes v, and the large kinetic energy of each molecule at $T > T_c$ results in rapid movement of molecules between the volumes v which corresponds to rapid flipping of the spins in the magnetic system. At these temperatures the size of fluid droplets is less than a critical value, insufficient to build long-range order because of the decreasing magnitude of the inter-molecular interaction. Additionally, at $T \gg T_c$, the fluid system approaches the ideal gas limit, where interactions between molecules can be neglected. On the other hand, at lower temperatures, the interacting molecules will form islands, a long-range order as in the magnetic system where the majority of spins prefer either up or down alignment. At the critical point, there will be a competition between the large islands ($\xi \to \infty$) of interacting molecules and macroscopic vacancies in volume V, resulting in a second-order transition from long-range order to short-range order. Even if the ρT phase diagram is not symmetric like the MT phase diagram, their equivalence at T_c is confirmed by the behaviour of the order parameter $\rho_{liquid} - \rho_{gas}$ of the fluid system and M of the magnetic system: In 3 dimensions, near the critical point, both order parameters depend on T as

$$O \sim (T - T_c)^{\beta} \,, \quad \beta \simeq \frac{1}{3} \,, \tag{1.6}$$

where O denotes the order parameter of the system in question. That is, approaching T_c

from the low-temperature side, the order parameters exhibit a power-law behavior with critical exponent β.

Each critical exponent is the same for fluid and magnetic systems. In general, one can find broad groups of systems which exhibit the same critical exponents, known as universality classes. Table 1.2 shows some of the universality classes with their corresponding critical exponents, among them the Ising, Potts[2], Heisenberg[3], and $X-Y$[4] classes. According to Table 1.2, both magnetic and fluid systems belong to $3D$ Ising universality class.

Universality class	α	β	γ	δ	ν	η
2D Ising	0(log)	1/8	7/4	15	1	1/4
3D Ising	0.1	0.33	1.24	4.8	0.63	0.04
3D X-Y	0.01	0.34	1.3	4.8	0.66	0.04
3D Heisenberg (mean-field)	−0.12	0.36	1.39	4.8	0.71	0.04
2D Potts, q=3	1/3	1/9	13/9	14	5/6	4/15
2D Potts, q=4	2/3	1/12	7/6	15	2/3	1/4

Table 1.2: Some of the universality classes [4].

1.2 Renormalization-Group Theory

Assigning critical exponents to the thermodynamic functions and building universality classes with respect to them gave researchers a better understanding of phase transitions and critical phenomena. However new questions arose in the 1960's: what is the underlying reason why second-order transitions fall into universality classes, how exponent equalities arise, how critical exponents take the same value as T_c is approached from above or below, and how the critical exponents depend on the spatial dimension of the system [4]. A theory which describes exactly what is happening near and at the critical point should also answer these questions.

[2]The Potts model with q states is the most general version of the Ising model. The energy of the system decreases when neighboring sites have equal states.

[3]In the classical Heisenberg model, a spin can take an arbitrary orientation in a unit sphere, and parallel alignments at neighboring sites decrease the energy of the system.

[4]Similar to the classical Heisenberg model, but with two dimensional spin vectors in a unit circle.

1.2.1 Scaling Theory of Kadanoff

The first attempt was made by Leo P. Kadanoff in 1966 [6], where he linearized the flows of the parameters under scale change, which map a thermodynamic system to another, equivalent thermodynamic system with less degrees of freedom, in the parameter space near the critical point by writing down recursion relations, for a magnetic system of the form

$$t' = b^{y_t} t\,, \quad \text{where} \quad t \equiv \frac{T - T_c}{T_c}\,, \tag{1.7}$$

$$H' = b^{y_H} H\,, \tag{1.8}$$

where t is reduced temperature, H is the magnetic field, b is the length rescaling factor, and the exponents y_t and y_H determine the dependence of linearized recursion relations on b. In position space, the procedure for obtaining these relations is as follows: Divide the lattice into cells of length b, giving clusters of b^d sites, where d is the dimension of the lattice. Select the alignment of the majority of the spins and replace each cell by a new spin variable s'_i with this alignment eliminating the degrees of freedom of $b^d - 1$ spins. The new system will have $N' = N/b^d$ spins. The essential condition for making the new system thermodynamically equivalent to the original one is that the partition function must be preserved,

$$Z_{N'}(\mathcal{H}') = \mathcal{Z}_{\mathcal{N}}(\mathcal{H})\,, \tag{1.9}$$

where $\mathcal{H}$ and $\mathcal{H}'$ denote the Hamiltonians of original and rescaled systems, respectively. This kind of transformation maps a point (t, H) to another point $(t'(t, H), H'(t, H))$ in the parameter space, where the primed variables refer to the parameters of the rescaled system. The rescaled system has a Hamiltonian of the same form as the original system, but with different parameters t' and H'. If this transformation is iterated, the successive mappings result in a flow in the parameter space. Additionally, the length scale of the system will change such that any quantity $\vec{r}$ with dimensions of length will be transformed as

$$\vec{r} \Rightarrow \vec{r}' = b^{-1}\vec{r}, \tag{1.10}$$

in the units of lattice spacing.

The flows in the parameter space are governed by fixed points where the system is invariant under a rescaling. At a fixed point, we have two equations for the correlation

length ξ, namely,

$$\xi' = b^{-1}\xi\,, \quad \text{and} \tag{1.11}$$

$$\xi' = \xi \equiv \xi^*\,. \tag{1.12}$$

There are two solutions for the correlation length ξ: $\xi = 0$ (trivial solution) or $\xi \to \infty$ (critical point).

For a magnetic system with recursion relations given in Equations 1.7 and 1.8, the point in the parameter space where $\xi \to \infty$ is $(t, H) = (0, 0)$, which is the critical point in Fig. 1.2 (a). Around $t = H = 0$ one can linearize $t'(t, H)$ and $H'(t, H)$, in order to obtain the recursion relations 1.7 and 1.8.

The critical exponents can be derived from Kadanoff's scaling theory. For instance, the scaling form of the dimensionless free energy per particle $f = \frac{1}{N}\log Z$ can be calculated near the critical point in order to obtain the exponent α. The partition function should be preserved, so:

$$f(t, H) = b^{-d} f(t', H') = b^{-d} f(b^{y_t} t, b^{y_H} H)\,, \tag{1.13}$$

In order to find the exponent α which is defined in the thermal direction, that is, approaching the critical point by varying $t(T)$ and keeping $H = 0$ constant, one can choose $b = t^{-1/y_t}$ which leads to

$$f(t, H) \sim t^{d/y_t}\,, \tag{1.14}$$

at $H = 0$, that is, approaching the critical point from the thermal direction. f scales like[5] $f \sim t^{2-\alpha}$, which gives $\alpha = 2 - \frac{d}{y_t}$.

The scaling theory of Kadanoff was successful in explaining phenomena near and at the critical point. However, it did not provide any method to calculate quantities away from criticality. Furthermore, it did not introduce any way of determining the recursion relations. These two issues were solved in K. G. Wilson's later work [7].

[5]Taking the second derivative of f over T, the factor 2 in the exponent is canceled, and the specific heat C_v is obtained, which scales like $C_v \sim t^{-\alpha}$ as given in Table 1.1.

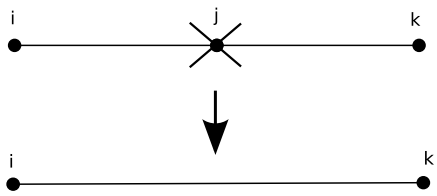

Figure 1.3: The decimation procedure with length rescaling factor $b = 2$ in the one-dimensional chain. The renormalized system consists of N/b sites.

1.2.2 The Renormalization Group

In 1971, the work of K. G. Wilson describing the momentum-space renormalization group[6] was a breakthrough, showing that the recursion relations were analytic and could be calculated for systems away from criticality. The method was applied to position space by Nelson and Fisher in 1975 [8].

For a one-dimensional Ising chain with periodic boundary conditions, the transformation can be done exactly by summing over half of the degrees of freedom of the system, as in fig. 1.3, while preserving the partition function Z, which leads to the recursion relations for all length scales. The original Hamiltonian of the system is

$$-\beta\mathcal{H} = J\sum_{\langle ij\rangle} s_i s_j + H\sum_i s_i\,, \tag{1.15}$$

where $\beta = 1/k_BT$, s_i is the spin variable, J the interaction constant between spins, and H is external magnetic field, is mapped to

$$-\beta'\mathcal{H}' = J'\sum_{\langle i'j'\rangle} s_{i'}s_{j'} + H'\sum_{i'} s_{i'} + \tilde{G}\,. \tag{1.16}$$

Here, the subscripts i' and j' refer to the indices of each of N' spins in the renormalized system. The closed-form recursion relations are $J'(J,H)$, $H'(J,H)$, and $\tilde{G}(J,H)$, where $\tilde{G}$ is the additive constant which contributes the free energy. Analysis of the recursion relations yields the fixed points $(J^*,H^*) = (0,0)$ and $(J^*,H^*) = (\infty,0)$ where the latter is the critical point.

RG transformations in higher dimensions can be formulated using methods such as cluster or Migdal-Kadanoff approximation procedures, which we shall use in Chapter 2.

[6]The momentum-space renormalization group transformation is performed by integrating out large wavevectors in $\vec{k}$-space, where $\vec{k}$ is the wavevector, and the Hamiltonian of the system is a function of all possible $\vec{k}$.

Consider the linear recursion relations in Eqs. 1.7 and 1.8 generating a flow near a fixed point in parameter space. The two exponents y_t and y_H control the behavior of an RG flow near the fixed point: If, for instance, $y_t < 0$, the fixed point is said to be stable in that direction[7] since the scaling field t drives the system to the fixed point. In contrast, when $y_t > 0$, the scaling field t drives the system away from the fixed point. In this case, the fixed point is said to be unstable in that direction[8][4]. When the exponents of all linearly independent parameters in the parameter space are negative, the fixed point is completely stable, and its basin of attraction is a thermodynamic phase. Thus, it is called a phase sink. On the other hand, when there is at least one unstable direction[9], the fixed point governs a phase boundary between thermodynamic phases.

1.3 Spin Glasses

Atoms are located randomly throughout a glass, and in contrast to the liquid-solid transition where atoms rearrange into a crystal structure, the rearranging time of the atoms in a glass into a crystal structure diverges upon cooling, known as the divergence of the relaxation time. At a critical temperature T_c called glass transition temperature, they become frozen in a spatial random configuration, because of diverging free energy barriers to relaxation [5]. This kind of phenomenon also applies to disordered lattice systems with nonuniform interactions between lattice sites where frustration occurs, leading to spin glasses, a phase with spins frozen in random orientations [9]. Frustration is competition between ferromagnetic and antiferromagnetic interactions. For instance, a loop with an odd number of antiferromagnetic (AF) interactions leads to frustration since one of the spins will have an unstable state [5].

For a disordered system with non-uniform interaction strengths between the lattice sites, the most general Hamiltonian for nearest-neighbor (nn) interactions between Ising spins is given by

$$H = -\sum_{\langle ij \rangle} J_{ij} s_i s_j \,, \tag{1.17}$$

[7]When the fixed point is stable in the direction of the flows, the field is called an irrelevant field.

[8]When the fixed point is unstable in the direction of the flows, the field is called a relevant field.

[9]There is a third possibility, $y_t = 0$, where the field is said to be marginal, and higher order terms become important in the analysis of the flows.

where $s_i = \pm 1$. Eq. 1.17 is called the Edwards-Anderson model. It is also known as the Ising spin glass (SG) model. Each J_{ij} is distributed identically and independently according to a multinomial distribution. Since the study of the spin glasses is complicated, the distribution function is usually assumed to have a simple form, for example:

$$P(J_{ij}) = p\delta(J_{ij} - J) + (1-p)\delta(J_{ij} + J)\,, \tag{1.18}$$

$$\text{or} \quad P(J_{ij}) = \frac{1}{\sqrt{2\pi J^2}} \exp\left(-\frac{(J_{ij} - J_0)^2}{2J^2}\right). \tag{1.19}$$

Eq. 1.18 is the $\pm J$ model where $J_{ij} = J$ (F coupling) with probablity p, or $J_{ij} = -J$ (AF coupling) with probablity $1-p$, for $J > 0$, whereas eq. 1.19 is the Gaussian model with mean J_0 and variance J^2 [9].

Thermodynamic quantities $\bar{Q}(\{J_{ij}\})$ depend on the specific configuration of interaction strengths $\{J_{ij}\}$ in the system, but to understand the physical properties of the system, one typically looks at the configurational average $\bar{Q}$, which is independent of $\{J_{ij}\}$:

$$[\bar{Q}] = \int \prod_{\langle ij \rangle} dJ_{ij} P\left(J_{ij}\right) \bar{Q}(\{J_{ij}\})\,. \tag{1.20}$$

In Section 3, we will give a method for the exact calculation of the site-dependent magnetization $m \equiv \langle s_i \rangle$ and the spin-glass order parameter $q \equiv \langle s_i^2 \rangle$ as a function of bond set $\{J_{ij}\}$, which can be applied to other thermodynamic quantities as well.

Chapter 2

QUANTUM SPIN-GLASS SYSTEMS

2.1 Quantum-Mechanically Induced Asymmetry in the Phase Diagrams of Spin-Glass Systems

A conspicuous finite-temperature effect of quantum mechanics is the critical temperature differentiation between ferromagnetic and antiferromagnetic systems.[10, 11, 12, 13] This is a contrast to classical systems where, *e.g.*, on loose-packed lattices ferromagnetic and antiferromagnetic systems are mapped onto each other and therefore have the same critical temperature. We find that this quantum effect is compounded and even more robust in spin-glass systems, which incorporate the passage from ferromagnetism and antiferromagnetism via quenched disorder.

Thus, in the present work, the phase diagrams of the spin-1/2 quantum Heisenberg spin-glass systems are calculated in all dimensions $d \geq 3$. In the space of temperature T and concentration p of antiferromagnetic bonds, remarkably asymmetric phase diagrams are obtained, in very strong contrast to the corresponding classical systems. Whereas, in the limit of $d \to \infty$, the differentiation of the critical temperatures of the ferromagnetic and antiferromagnetic pure systems disappears, the Tp phase diagrams remain strongly asymmetric at low but finite temperatures, where quantum fluctuations remain dominant independent of dimensionality. A direct second-order phase boundary between ferromagnetic and antiferromagnetic phases, not seen in classical systems, is found in $d > 5$. In lower d, a paramagnetic phase intervenes between the ferromagnetic and antiferromagnetic systems. Our calculation is an approximation for hypercubic lattices and, simultaneously, a lesser approximation for hierarchical lattices [14, 15, 16, 17, 18, 19, 20, 21, 22, 23, 24].

The spin-1/2 quantum Heisenberg spin-glass systems have the Hamiltonian $-\beta\mathcal{H} = \sum_{\langle ij \rangle} J_{ij}\mathbf{s}_i \cdot \mathbf{s}_j \equiv \sum_{\langle ij \rangle} -\beta\mathcal{H}(i,j)$, where $\langle ij \rangle$ denotes a sum over pairs of nearest-neighbor sites. J_{ij} is equal to the ferromagnetic value of $J > 0$ with probability $1 - p$ and to the antiferromagnetic value of $-J < 0$ with probability p. We solve this model by extending the

Suzuki-Takano rescaling [25, 26, 12, 30, 31, 13, 32, 27, 28, 29, 33] to non-uniform systems and to length-rescaling factor $b = 3$, necessary for the *a priori* equivalent treatment of ferromagnetism and antiferromagnetism, followed by the essentially exact treatment [34, 35] of the quenched randomness giving the non-uniformity. In one dimension,

$$\begin{aligned} \mathrm{Tr}_{(j,k)} e^{-\beta\mathcal{H}} &= \mathrm{Tr}_{(j,k)} e^{\sum_i^{4\mathrm{n}} \{-\beta\mathcal{H}(i,j)-\beta\mathcal{H}(j,k)-\beta\mathcal{H}(k,l)\}} \\ &\simeq \prod_i^{4\mathrm{n}} \mathrm{tr}_{(j,k)} e^{\{-\beta\mathcal{H}(i,j)-\beta\mathcal{H}(j,k)-\beta\mathcal{H}(k,l)\}} \\ &= \prod_i^{4\mathrm{n}} e^{-\beta'\mathcal{H}'(i,l)} \simeq e^{\sum_i^{4\mathrm{n}} \{-\beta'\mathcal{H}'(i,l)\}} = e^{-\beta'\mathcal{H}'}, \end{aligned} \tag{2.1}$$

where the sums and products i are over every fourth spin along the chain, the traces are over all other spins, and $-\beta'\mathcal{H}'$ is the renormalized Hamiltonian. Thus, the commutation rules are correctly accounted for within four-site segments, at all successive length scales in the iterations of the renormalization-group transformation. The trace tr is performed by quantum algebra, as given below.

The rescaling is extended to dimensions $d > 1$ by bond-moving, namely by adding b^{d-1} interactions resulting from the decimation of Eq.(1.4), to obtain the renormalized interaction strength $J'_{i'j'} = R(\{J_{ij}\})$, where $\{J_{ij}\}$ includes b^d interactions of the unrenormalized system. The interaction constant values $\{J_{ij}\}$ are distributed with a quenched probability distribution $\mathcal{P}(J_{ij})$ [34, 35], which starts out as a double-delta function but quickly becomes complicated under its renormalization-group transformation, given by the convolution $\mathcal{P}'(J'_{i'j'}) = \int [\prod_{ij}^{i'j'} dJ_{ij}\, \mathcal{P}(J_{ij})] \delta(J'_{i'j'} - R(\{J_{ij}\}))$. This equation actually involves b^d convolutions (for example, 729 convolutions for the $d = 6$ system discussed below), which are constituted of triplet convolutions of interactions in series (decimation) and pairwise convolutions of interactions in parallel (bond-moving). The quenched probability distribution $\mathcal{P}(J_{ij})$ is kept numerically in terms of histograms. The number of histograms multiplicatively increases under rescaling, until a calculationally acceptable maximum is reached. After this point, the number of histograms is kept constant by implementing a binning procedure before each pairwise or triplet convolution. We employ a new binning procedure, in which bins are demarked so as to contain equal probabilities, as opposed to equal interaction intervals as done previously. Starting from the lowest J value and moving to greater ones,

histograms in each consecutive bin are combined, to interaction value $J = \Sigma p_i J_i / \Sigma p_i$ and imposed equal probability $p = \Sigma p_i = 1/n_{\rm bin}$. In this process, histograms at the boundaries of bins are apportioned between the consecutive bins. Thus, our calculation has 125,000 histograms after each decimation and 40,000 histograms after each pairwise bond moving. The global flows of the quenched probability distributions yield the phase diagrams. Analysis of the unstable fixed points and unstable fixed distributions attracting the phase boundaries yields the order of the phase transitions.

Calculations are done for the quantum Heisenberg spin-glass systems in integer dimensions. No finite-temperature phase transition occurs in $d = 1, 2$. The phase diagrams for $d = 3, 4, 5, 6, 8, 10$ are shown in Fig.2.1. They are all strikingly asymmetric, especially in the middle p and low-temperature (would-be spin-glass phase) region. In $d = 3$, our calculated ratio of the critical temperatures of the pure antiferromagnetic and ferromagnetic systems is $T_C^{AF}/T_C^F = 1.48$. This value is to be compared with the values of 1.13 found in the cubic lattice [10, 11] and 1.22 found in the $b = 2, d = 3$ hierarchical lattice [12, 13]. This critical temperature difference is consistent with the lower ground-state energy of the antiferromagnetic system, as calculated [9] in $d = 3$. Our calculated ratios of the antiferromagnetic and ferromagnetic critical temperatures, for $d = 4, 5, 6, 8, 10$, decrease as 1.22, 1.12, 1.07, 1.02, 1.01 respectively. On the other hand, it is seen that although the phase boundaries leading to the pure ferromagnetic and antiferromagnetic critical points regain symmetry as d is increased, the low-temperature phase diagrams remain asymmetric. The ferromagnetic phase penetrates the antiferromagnetic region at low temperatures. Thus, quantum fluctuations present at low temperatures favor the ferromagnetic phase over the antiferromagnetic phase. In $d \geq 6$, a second-order phase boundary occurs directly between the ferromagnetic and antiferromagnetic phases, as is not seen in classical spin-glass systems. A new multicritical point occurs where all three second-order boundaries meet.

The phase transition, between ordered phases, that is driven by quenched randomness presents a contrast to phase transitions between ordered phases driven by a systemwise uniform interaction. The latter phase transition is obtained, at low temperatures, by driving a uniform interaction that favors another ordered phase over the existing one. Under these conditions, essentially the entire system remains in one ordered phase until the phase transition point is reached, when essentially the entire system changes over to the other phase.

Throughout this process, the ordered domains are compact and have fractal dimensionality equal to spatial dimensionality, which translates to having a renormalization-group eigenvalue exponent of $y = d$, the condition for a first-order transition [37]. By contrast, the phase transition with quenched randomness is obtained, at low temperatures, by driving quenched local interactions that favor the other ordered phase over the existing phase. This means, for example, increasing the number of random antiferromagnetic bonds when the system is in the ferromagnetic phase. Under these conditions, the ferromagnetic domains avoid the random localities of antiferromagnetic bonds in the system. The ferromagnetically ordered domains loose weight as the transition is approached, so that the average magnetization decreases. At the phase transition, the ordered domains are not compact and have fractal dimensionality less than the spatial dimensionality, so that the magnetization is zero. This translates to the renormalization-group eigenvalue exponent $y < d$, meaning a second-order phase transition. The converse happens when the phase transition is approached from the opposite side, with non-compact antiferromagnetic domains avoiding the random localities of the ferromagnetic bonds. Thus, we find that whereas phase transitions between ordered phases are first order when driven by a uniform interaction, they are second order when driven by quenched randomness.

In $d = 3, 4, 5$, the paramagnetic phase reaching zero temperature (as an extremely narrow sliver in $d = 5$) intervenes between the ferromagnetic and antiferromagnetic phases. In all cases, the ferromagnetic phase penetrates, reaching the high p values of 0.63 and 0.83 respectively in $d = 3$, where there is a zero-temperature paramagnetic interval, and $d \geq 4$, where there is no zero-temperature paramagnetic interval. The antiferromagnetic phase recedes at low temperatures, thereby showing a reentrant phase boundary [35].

There is no spin-glass phase, in the quantum system, in any dimension. The quantum version of the Sherrington-Kirkpatrick model [38], namely the spin-1/2 quantum Heisenberg model with equivalent-neighbor interactions, with a symmetric gaussian distribution, studied from the high-temperature side, yields a finite-temperature phase transition, which has been interpreted as a transition to a low-temperature spin-glass phase [39]. This model should be similar to our studied models at $p = 0.5$ in the large d limit. Thus, we also find a finite-temperature phase transition (Fig.2.1), but the low-temperature phase is explicitly a ferromagnetic phase with quenched bond randomness. The latter phase has considerable

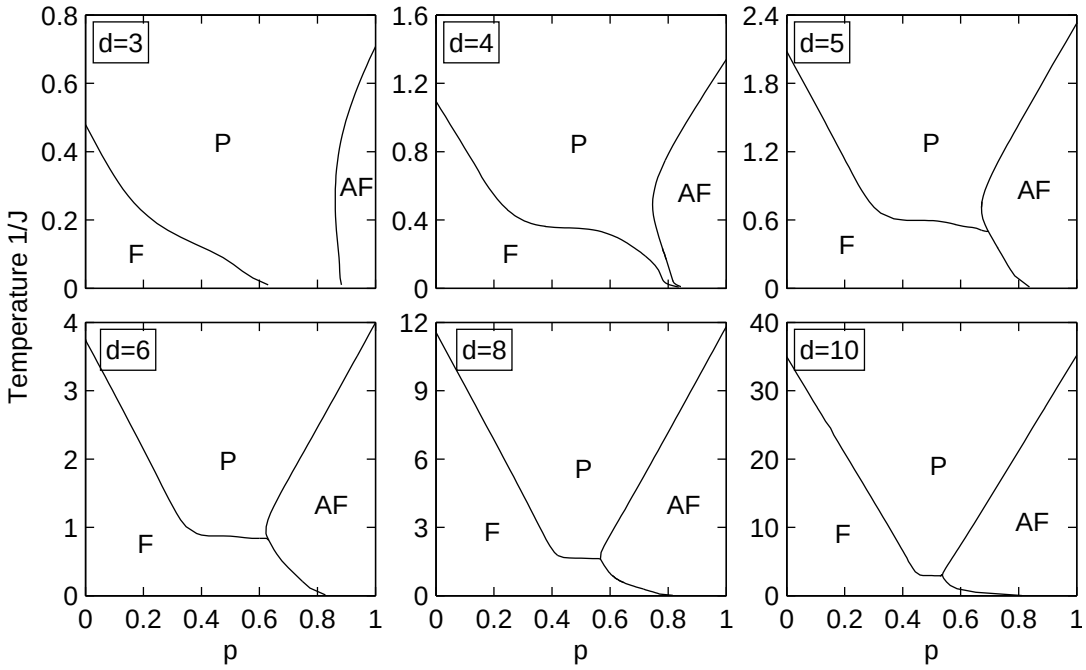

Figure 2.1: Phase diagrams of the quantum Heisenberg spin-glass systems in temperature $1/J$ versus antiferromagnetic bond concentration p for $d = 3$ to 10. All transitions are second-order, between the ferromagnetic (F), antiferromagnetic (AF), and paramagnetic (P) phases.

amount of short-range antiferromagnetic correlations, as seen in Ref.[40].

2.2 Appendix

The operators $-\beta'\mathcal{H}'(i,l)$ and $-\beta\mathcal{H}(i,j) - \beta\mathcal{H}(j,k) - \beta\mathcal{H}(k,l)$ of Eq. 2.1 act on two-site and four-site states, respectively, where at each site the spin is in quantum state $\sigma = \uparrow$ or $\downarrow$. The trace tr in Eq. 2.1 is, in terms of matrix elements [12],

$$\langle u_i z_l | e^{-\beta'\mathcal{H}'(i,l)} | \bar{u}_i \bar{z}_l \rangle = \sum_{v_j, w_k} \langle u_i \, v_j \, w_k z_l | e^{-\beta\mathcal{H}(i,j) - \beta\mathcal{H}(j,k) - \beta\mathcal{H}(k,l)} | \bar{u}_i \, v_j \, w_k \bar{z}_l \rangle \, , \tag{2.2}$$

where $u_i, v_j, w_k, z_l, \bar{u}_i, \bar{z}_l$ are single-site state variables. Thus, Eq. 2.2 is the contraction of a 16×16 matrix into a 4×4 matrix. Basis states that are simultaneous eigenstates of parity (p), total spin magnitude (s), and total spin z-component (m_s) block-diagonalize these matrices and thereby make Eq. 2.2 manageable. These sets of 4 two-site and 16 four-site eigenstates, denoted by $\{|\phi_p\rangle\}$ and $\{|\psi_q\rangle\}$ respectively, are given in Tables I and

p	s	m_s	Two-site eigenstates
$+$	1	1	$\|\phi_1\rangle = \|\uparrow\uparrow\rangle$
$+$	1	0	$\|\phi_2\rangle = \frac{1}{\sqrt{2}}\{\|\uparrow\downarrow\rangle + \|\downarrow\uparrow\rangle\}$
$-$	0	0	$\|\phi_4\rangle = \frac{1}{\sqrt{2}}\{\|\uparrow\downarrow\rangle - \|\downarrow\uparrow\rangle\}$

Table 2.1: The two-site basis states, with the corresponding parity (p), total spin (s), and total spin z-component (m_s) quantum numbers. The state $|\phi_3\rangle$ is obtained by spin reversal from $|\phi_1\rangle$. The renormalized two-site Hamiltonian $-\beta' H'(i,l)$ is diagonal in this set, with the diagonal elements of $|\phi_{1-3}\rangle$ and $|\phi_4\rangle$ being $\frac{1}{4}J' + G'$ and $-\frac{3}{4}J' + G'$ respectively.

II. The diagonal blocks are given in Tables I and III. Due to the microscopic randomness of the spin-glass problem, the four-site Hamiltonian mixes states of different parity, as seen in Table IV. Eq. 2.2 is thus rewritten as

$$\begin{aligned}\langle\phi_p|e^{-\beta'\mathcal{H}'(i,k)}|\phi_{\bar{p}}\rangle \quad &= \textstyle\sum_{u,z,\bar{u},\bar{z},v,w}\sum_{q,\bar{q}}\langle\phi_p|u_i z_l\rangle\langle u_i v_j w_k z_l|\psi_q\rangle \times \\ &\langle\psi_q|e^{-\beta\mathcal{H}(i,j)-\beta\mathcal{H}(j,k)-\beta\mathcal{H}(k,l)}|\psi_{\bar{q}}\rangle\langle\psi_{\bar{q}}|\bar{u}_i v_j w_k \bar{z}_l\rangle\langle\bar{u}_i\bar{z}_l|\phi_{\bar{p}}\rangle\ .\end{aligned} \tag{2.3}$$

There are only two rotation-symmetry independent elements of $\langle\phi_p|e^{-\beta'\mathcal{H}'(i,l)}|\phi_{\bar{p}}\rangle \equiv \langle\phi_p||\phi_{\bar{p}}\rangle$ in Eq.2.3, which have $p = \bar{p} = 1, 4$ (thereby leading to one renormalized interaction constant J' and the additive constant G'). From Eq. 2.3, $\langle\phi_1||\phi_1\rangle = \langle\psi_1||\psi_1\rangle + \frac{1}{2}\langle\psi_2||\psi_2\rangle + \frac{1}{6}\langle\psi_3||\psi_3\rangle + \frac{1}{2}\langle\psi_6||\psi_6\rangle + \frac{1}{2}\langle\psi_7||\psi_7\rangle + \frac{1}{2}\langle\psi_9||\psi_9\rangle - \langle\psi_9||\psi_{10}\rangle + \frac{1}{2}\langle\psi_{10}||\psi_{10}\rangle + \frac{1}{3}\langle\psi_{16}||\psi_{16}\rangle$ and $\langle\phi_4||\phi_4\rangle = \langle\psi_9||\psi_9\rangle + 2\langle\psi_9||\psi_{10}\rangle + \langle\psi_{10}||\psi_{10}\rangle + \frac{1}{2}\langle\psi_{11}||\psi_{11}\rangle + \langle\psi_{11}||\psi_{12}\rangle + \frac{1}{2}\langle\psi_{12}||\psi_{12}\rangle + \langle\psi_{15}||\psi_{15}\rangle$, with $\langle\psi_q||\psi_{\bar{q}}\rangle \equiv \langle\psi_q|e^{-\beta\mathcal{H}(i,j)-\beta\mathcal{H}(j,k)-\beta\mathcal{H}(k,l)}|\psi_{\bar{q}}\rangle$. From Table I, the renormalized interaction constant is given by $J' = \ln(\langle\phi_1||\phi_1\rangle/\langle\phi_4||\phi_4\rangle)$.

p	s	m_s	Four-site eigenstates
$+$	2	2	$\|\psi_1\rangle = \|\uparrow\uparrow\uparrow\uparrow\rangle$
$+$	2	1	$\|\psi_2\rangle = \frac{1}{2}\{\|\uparrow\uparrow\uparrow\downarrow\rangle + \|\uparrow\uparrow\downarrow\uparrow\rangle + \|\uparrow\downarrow\uparrow\uparrow\rangle + \|\downarrow\uparrow\uparrow\uparrow\rangle\}$
$+$	2	0	$\|\psi_3\rangle = \frac{1}{\sqrt{6}}\{\|\uparrow\uparrow\downarrow\downarrow\rangle + \|\uparrow\downarrow\uparrow\downarrow\rangle + \|\uparrow\downarrow\downarrow\uparrow\rangle$ $+\|\downarrow\uparrow\uparrow\downarrow\rangle + \|\downarrow\uparrow\downarrow\uparrow\rangle + \|\downarrow\downarrow\uparrow\uparrow\rangle\}$
$+$	1	1	$\|\psi_6\rangle = \frac{1}{2}\{\|\uparrow\uparrow\uparrow\downarrow\rangle - \|\uparrow\uparrow\downarrow\uparrow\rangle - \|\uparrow\downarrow\uparrow\uparrow\rangle + \|\downarrow\uparrow\uparrow\uparrow\rangle\}$
$+$	1	0	$\|\psi_7\rangle = \frac{1}{\sqrt{2}}\{\|\downarrow\uparrow\uparrow\downarrow\rangle - \|\uparrow\downarrow\downarrow\uparrow\rangle$
$-$	1	1	$\|\psi_9\rangle = \frac{1}{2}\{\|\uparrow\uparrow\uparrow\downarrow\rangle - \|\uparrow\uparrow\downarrow\uparrow\rangle + \|\uparrow\downarrow\uparrow\uparrow\rangle - \|\downarrow\uparrow\uparrow\uparrow\rangle\}$ $\|\psi_{10}\rangle = \frac{1}{2}\{\|\uparrow\uparrow\uparrow\downarrow\rangle + \|\uparrow\uparrow\downarrow\uparrow\rangle - \|\uparrow\downarrow\uparrow\uparrow\rangle - \|\downarrow\uparrow\uparrow\uparrow\rangle\}$
$-$	1	0	$\|\psi_{11}\rangle = \frac{1}{\sqrt{2}}\{\|\uparrow\downarrow\uparrow\downarrow\rangle - \|\downarrow\uparrow\downarrow\uparrow\rangle$ $\|\psi_{12}\rangle = \frac{1}{\sqrt{2}}\{\|\uparrow\uparrow\downarrow\downarrow\rangle - \|\downarrow\downarrow\uparrow\uparrow\rangle$
$+$	0	0	$\|\psi_{15}\rangle = \frac{1}{2}\{\|\uparrow\uparrow\downarrow\downarrow\rangle - \|\uparrow\downarrow\uparrow\downarrow\rangle - \|\downarrow\uparrow\downarrow\uparrow\rangle + \|\downarrow\downarrow\uparrow\uparrow\rangle\}$ $\|\psi_{16}\rangle = \frac{1}{\sqrt{12}}\{\|\uparrow\uparrow\downarrow\downarrow\rangle + \|\uparrow\downarrow\uparrow\downarrow\rangle - 2\|\uparrow\downarrow\downarrow\uparrow\rangle$ $-2\|\downarrow\uparrow\uparrow\downarrow\rangle + \|\downarrow\uparrow\downarrow\uparrow\rangle + \|\downarrow\downarrow\uparrow\uparrow\rangle\}$

Table 2.2: The four-site basis states, with the corresponding parity (p), total spin (s), and total spin z-component (m_s) quantum numbers. The states $|\psi_{4,5}\rangle$, $|\psi_8\rangle$, $|\psi_{13,14}\rangle$ are obtained by spin reversal from $|\psi_{2,1}\rangle$, $|\psi_6\rangle$, $|\psi_{9,10}\rangle$, respectively.

	ψ_1	ψ_2	ψ_3
ψ_1	$\frac{1}{4}(J_1+J_2+J_3)$	0	0
ψ_2	0	$\frac{1}{4}(J_1+J_2+J_3)$	0
ψ_3	0	0	$\frac{1}{4}(J_1+J_2+J_3)$

	ψ_6	ψ_9	ψ_{10}
ψ_6	$\frac{1}{4}(-J_1+J_2-J_3)$	$\frac{1}{2}(J_1-J_3)$	0
ψ_9	$\frac{1}{2}(J_1-J_3)$	$-\frac{1}{4}(J_1+J_2+J_3)$	$\frac{1}{2}J_2$
ψ_{10}	0	$\frac{1}{2}J_2$	$\frac{1}{4}(J_1-J_2+J_3)$

	ψ_7	ψ_{11}	ψ_{12}
ψ_7	$\frac{1}{4}(-J_1+J_2-J_3)$	$\frac{1}{2}(J_1-J_3)$	0
ψ_{11}	$\frac{1}{2}(J_1-J_3)$	$-\frac{1}{4}(J_1+J_2+J_3)$	$\frac{1}{2}J_2$
ψ_{12}	0	$\frac{1}{2}J_2$	$\frac{1}{4}(J_1-J_2+J_3)$

	ψ_{15}	ψ_{16}
ψ_{15}	$-\frac{3}{4}J_2$	$\frac{\sqrt{3}}{4}(J_1+J_3)$
ψ_{16}	$\frac{\sqrt{3}}{4}(J_1+J_3)$	$\frac{1}{4}(-2J_1+J_2-2J_3)$

Table 2.3: Diagonal matrix blocks of the unrenormalized three-site Hamiltonian $-\beta H(i,j)-\beta H(j,k)-\beta H(k,l)$. The Hamiltonian being invariant under spin-reversal, the spin-flipped matrix elements are not shown. The additive constant $3G$ at the diagonal elements is not shown. The interaction constants J_1, J_2, J_3, which are in general unequal due to quenched randomness, are from $-\beta\mathcal{H}(i,j)$, $-\beta\mathcal{H}(j,k)$, $-\beta\mathcal{H}(k,l)$ respectively.

Chapter 3

APOLLONIAN SMALL-WORLD NETWORKS

Small-world networks were introduced in 1998 by Watts and Strogatz [41]. The defining characteristic of small-world networks is that the average shortest-path length scales like $\log N$, where N is the number of sites in the network.

Many real-life networks, such as the Internet [43, 44, 45], the collaboration graph of film actors, power grids [46], are small-world networks. In order to understand the dynamics behind social, biological, technological networks, various small-world network models have been developed to date: Watts and Strogatz's network [41] (WS network), Newman and Watts' network [49], hierarchical-lattice small-world networks proposed by Hinczewski and Berker [18], and Apollonian networks (AN) introduced by Andrade *et al.* [50] are a few examples. Among them, hierarchical-lattice small-world networks and AN's have an additional property: a power-law degree distribution which makes a network scale free, like in the well-known Barabàsi and Albert's network model [47, 48] (BA network) where preferential attachment occurs, in other words, growth of the network happens in such a way that new sites are preferentially attached to existing sites with large numbers of nearest neighbors. Usually, small-world networks have large clustering coefficients[1] like regular lattices, a measure of the network being highly clustered. In this chapter, we will focus on the thermodynamics of AN's.

There have been various studies on AN, dealing with both their statistical and thermodynamic properties. After the first study of AN [50], the same authors introduced the Random Apollonian Network (RAN) in Ref. [42], for which they calculated the statistical characteristics, as well as th behavior of percolation and epidemic spreading processes on the network. Oron *et al.* developed variations on the topology of AN. [54]. Zhang *et al.* calculated correlations in RAN [52] and introduced another AN class which is called

[1]The clustering coefficient $C(i)$ of a site i is the ratio between the number of bonds among the nearest-neighbor set $A(i)$ of site i and the total possible number $k_i(k_i-1)/2$, where k_i is the coordination number of site i, and the clustering coefficient C of the network is the average of $C(i)$ over all i [42].

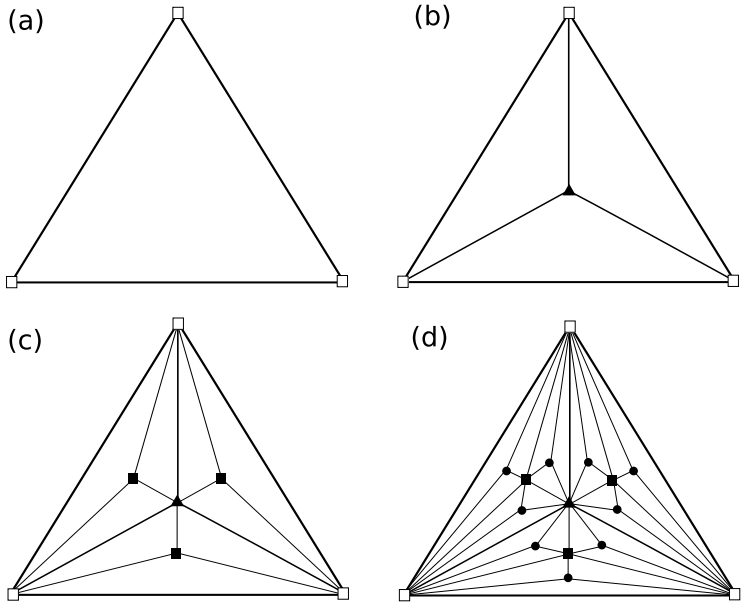

Figure 3.1: Construction of an Apollonian network. Empty boxes are the edges of the main triangle, whereas full triangles, full squares, and full circles are 1st, 2nd and 3rd generations, respectively. Following this procedure *ad infinitum*, an AN is obtained in the thermodynamic limit.

EAN (Evolutionary Apollonian Network), focusing on its statistical properties. In addition, correlated electron systems were studied on AN [55].

The network characteristics of AN can be summarized as follows: AN's are scale-free, that is, display a power-law degree distribution with $P(k) \sim k^{1-\gamma}$ [50] with $\gamma \simeq 2.585$, where k is the degree; they have small-world properties due to their short average shortest-path length $\bar{l} \sim \log N$ [51]; and they have a large clustering coefficient $\lim_{N\to\infty} C = 0.828$ [50].

Figure 3.1 shows the growth pattern of an AN. In this chapter, we look at the thermodynamics of the Edwards-Anderson model discussed in section 1.3 on an AN focusing on the percolation and spin-glass cases. The percolation examples which Ref. [42] investigates are random failures and intentional attacks on networks, which are first introduced by Albert *et al.* [56]. However, to date a site-percolation or bond-percolation of the Edwards-Anderson model is not studied on AN. Thus, we will examine a disordered system on a network with each sites having two states such as, for instance, whether the members of a social network share a common belief or not, or whether the nodes of a computer network are online or offline, etc.

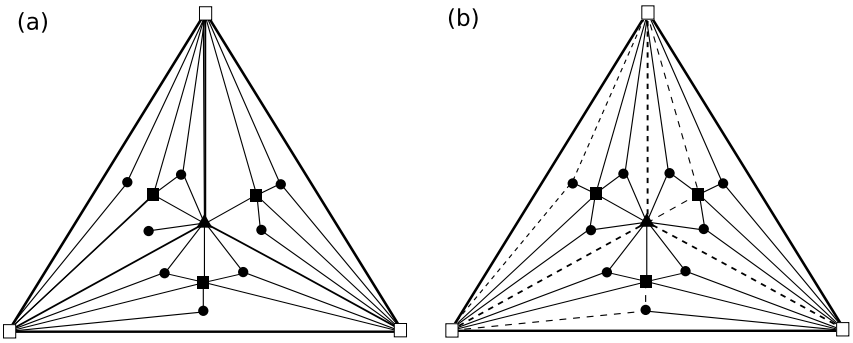

Figure 3.2: (a) Bond (edge) percolation on an AN. (b) A spin-glass system on an AN, where full bonds represent $J > 0$ (ferromagnetic coupling), and dashed bonds $J < 0$ (antiferromagnetic coupling).

The spin-1/2 Edwards-Anderson model is given by

$$-\beta H = \sum_{\langle ij \rangle} J_{ij} s_i s_j \,, \tag{3.1}$$

with a bond distribution for the spin-glass case

$$P(J_{ij}) = p\delta(J_{ij} + J) + (1-p)\delta(J_{ij} - J) \,, \tag{3.2}$$

where $J_{ij} = J > 0$ for F coupling with probability $1-p$, and $J_{ij} = -J$ for AF coupling with probability p. Similarly, for the bond-percolation case, the distribution function is

$$P(J_{ij}) = p\delta(J_{ij} - \tilde{J}) + (1-p)\delta(J_{ij}) \,, \tag{3.3}$$

where $J_{ij} = \tilde{J} = J$ for F bond-percolation and $J_{ij} = \tilde{J} = -J$ for AF bond-percolation, both with probability p, and $J_{ij} = 0$ with probability $1-p$ for both cases.

The hierarchical structure of AN allows us to form an exact renormalization-group transformation as follows: The crucial step of the RG transformation is the star-triangle transformation, which eliminates one site in the middle of the star, generating renormalized interactions among the three outer sites, as shown in Fig. 3.3(a). That is,

$$e^{-\beta' H'(s_1,s_2,s_3)} = \sum_{\sigma=\pm 1} e^{-\beta H(\sigma,s_1,s_2,s_3)} \tag{3.4}$$

generates the following recursion relations for a non-uniform system, which connect the original interaction constants of a star to the renormalized interaction constants of a triangle:

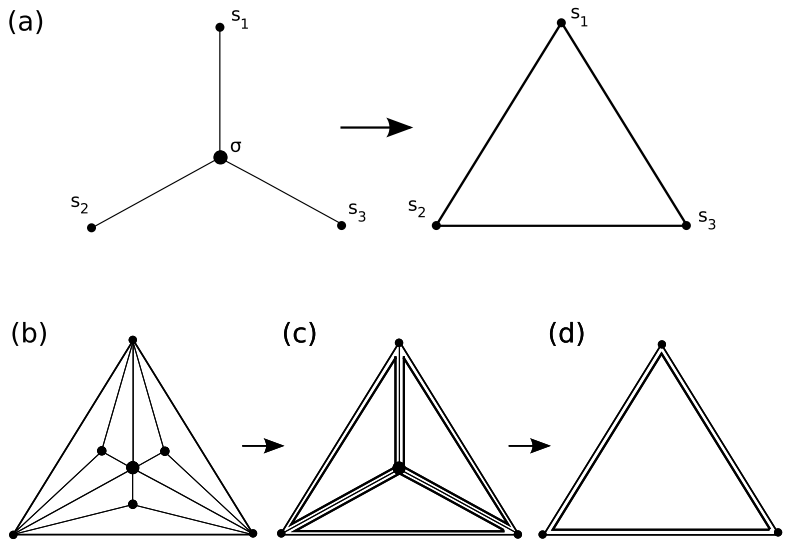

Figure 3.3: (a) The star-triangle transformation. (b) Decimation of three sites using the star-triangle transformation. (c) Another star-triangle transformation renormalizes the system to (d).

$$\tilde{J}_{13} = \frac{1}{4}\log\frac{\gamma_1\gamma_3}{\gamma_2\gamma_4}\,, \quad \tilde{J}_{23} = \frac{1}{4}\log\frac{\gamma_1\gamma_4}{\gamma_2\gamma_3}\,, \tag{3.5}$$
$$\tilde{J}_{12} = \frac{1}{4}\log\frac{\gamma_1\gamma_2}{\gamma_3\gamma_4}\,, \quad \tilde{G} = \frac{1}{4}\log\gamma_1\gamma_2\gamma_3\gamma_4\,,$$

where

$$\gamma_1 = 2\cosh(J_1+J_2+J_3)\,, \quad \gamma_2 = 2\cosh(J_1+J_2-J_3)\,, \tag{3.6}$$
$$\gamma_3 = 2\cosh(J_1-J_2+J_3)\,, \quad \gamma_4 = 2\cosh(-J_1+J_2+J_3)\,.$$

Here an original bond J_i refers to the bond between site i and σ, whereas the renormalized bond $\tilde{J}_{ij}$ refers to a contribution to the renormalized bond between sites i and j. As in fig. 3.3, before every decimation process, we combine the contributions that connect the same sites to each other, where $n = 2$ for the bigger triangle in Fig 3.3 (c) and (d), and $n = 3$ for the star in (c), ultimately leading to the triangle in (e).

In order to implement the renormalization group for a disordered system on an AN, we use Nobre's method. This method, applied to hierarchical lattices [14, 15, 16] by Nobre [57] and Ohzeki *et al.* [58], has been successful in determining the thermodynamic phases and multicritical points of the Ising spin glass. First, we produce a sample pool of 10^6 triangles

where each edge of a triangle follows one of the initial distributions in Eqs. 3.2 and 3.3, depending on the model. Then, randomly choosing three triangles from this initial pool repeatedly, we apply the RG transform on each triplet of triangles, until we have produced another pool of renormalized triangles of size 10^6. Note that at each step, the middle one of the three contributions on each arm of the star obeys the initial distribution, given by either Eq. 3.2 or 3.3.

Tracing out the states of decimated sites at each RG step corresponds to an inverse process of construction of an AN. RG flows are generated in an $3 \cdot 10^6$ dimensional space, leading to a multinomial distribution for each bond of each renormalized triangle in the pool. Keeping the renormalized triangle pool size on the order of $\sim 10^6$ allows us to locate the phase boundaries and other thermodynamic properties clearly, overcoming the computational difficulty in [58], which arises from lattices of finite size and finite number of bonds in the pool. We observe $[J_{ij}]$ and $\sigma_{J_{ij}} = \sqrt{[J_{ij}^2] - [J_{ij}]^2}$, where $[Q]$ is the configurational average of a renormalized quantity Q over the renormalized distribution. In our analysis of the flows, we realize that three scenarios arise:

$$\begin{aligned} \langle J_{ij} \rangle \to \infty \quad \text{and} \quad \frac{\sigma_{J_{ij}}}{\langle J_{ij} \rangle} \to 0\,, \quad \text{F phase}\,, \\ \langle |J_{ij}| \rangle \to \infty \quad \text{and} \quad \frac{\langle J_{ij} \rangle}{\sigma_{J_{ij}}} \to 0\,, \quad \text{SG-like phase}\,, \\ \langle J_{ij} \rangle \to 0 \quad \text{and} \quad \sigma_{J_{ij}} = 0\,, \quad \text{P phase}\,. \end{aligned} \tag{3.7}$$

The paramagnetic (P) phase only occurs for $p = 1$ in the AF bond-percolation model. In order to determine whether the phases which we call F and SG-like are in fact F and SG phases, we calculate the order parameters, that is, the ferromagnetic order parameter (magnetization) $M \equiv [m] \equiv [\langle s_i \rangle]$, and the spin-glass order parameter $Q \equiv [q] \equiv [\langle s_i \rangle^2]$. In an F phase, both order parameters should be finite, whereas in an SG phase, Q should be finite and M should vanish.

To calculate the magnetization and the SG order parameter, we add a magnetic field H_σ to site σ,

$$m = \left. \frac{\partial \log Z}{\partial H_\sigma} \right|_{H_\sigma = 0}\,, \tag{3.8}$$

which modifies the Hamiltonian of the system in Fig. 3.3 (a), such that

$$-\beta H(s_1, s_2, s_3, \sigma) = J_1 s_1 \sigma + J_2 s_2 \sigma + J_3 s_3 \sigma + H_\sigma \sigma + K s_2 s_3 \sigma\,, \tag{3.9}$$

where K is a three-site interaction which is generated by an original Hamiltonian with only $\{J_i, H_\sigma\}$ terms upon renormalization. Mathematically, when adding an H_σ term, adding K makes the RG-space closed under repeated iterations, since the number of independent variables are equal to the number of linearly independent γ_i . Then,

$$m = \left[\frac{\partial \log Z}{\partial H_\sigma}\right]_{H_\sigma=0} = \left[\frac{\partial \log Z}{\partial K'_\alpha}\right]_{K'_\alpha=0} \left[\frac{\partial K'_\alpha}{\partial H_\sigma}\right]_{H_\sigma=0} \quad \text{where} \quad K'_\alpha = \{H'_1, H'_2, H'_3, K'\} \,, \tag{3.10}$$

in terms of renormalized interaction constants K'_α, where summation over repeated indices is implicit. Under repeated iterations, eq. 3.10 becomes

$$m = \frac{\partial \log Z}{\partial K_\delta^{(n)}} \frac{\partial K_\delta^{(n)}}{\partial K_\gamma^{(n-1)}} \cdots \frac{\partial K_\beta^{(2)}}{\partial K_\alpha^{(1)}} \frac{\partial K_\alpha^{(1)}}{\partial H_\sigma} \,, \tag{3.11}$$

where $K_\alpha^{(i)} = 0$ for all derivatives. In order to reach the fixed point, the $n \to \infty$ limit should be taken, which is necessary for calculating the thermodynamic densities. In closed form, eq. 3.11 can be rewritten as

$$m^{(0)} = \mu^{(\mathbf{n})}{}_{1\times 4} \mathbf{T}^{(\mathbf{n})}{}_{4\times 4} \mathbf{T}^{(\mathbf{n-1})}{}_{4\times 4} \ldots \mathbf{T}^{(\mathbf{2})}{}_{4\times 4} \mathbf{V}^{(\mathbf{1})}{}_{4\times 1} \,, \tag{3.12}$$

where the subscripts refer to the dimensions of the matrices $\mathbf{T}^{(\mathbf{i})}$ and vectors $\mu^{(\mathbf{n})}$, $\mathbf{V}^{(\mathbf{1})}$, defined as:

$$\mu^{(\mathbf{n})} \equiv \frac{\partial \log Z}{\partial K_\delta^{(n)}} \,, \quad \mathbf{T}^{(\mathbf{i})} \equiv \frac{\partial K_\beta^{(i)}}{\partial K_\alpha^{(i-1)}} \,, \quad \text{and} \quad \mathbf{V}^{(\mathbf{1})} \equiv \frac{\partial K_\alpha^{(1)}}{\partial H_\sigma} \,. \tag{3.13}$$

In order to obtain a finite magnetization, one should take the limits[2] $\lim_{H\to 0} \lim_{N\to\infty} M$ where N is the number of sites. The system should be renormalized until reaching the phase sink, where the analysis of the eigenvalues and left eigenvectors of $\mathbf{T}^{(\mathbf{i})}$, together with Eq. 3.12 lets us calculate the site-dependent magnetization of the original system. However, in the SG-like phase, it is difficult to reach the phase sink, yet we can clearly identify the SG-like phase since $[J_{ij}]/\sigma_{J_{ij}} \to 0$. On the other hand, $\left.\frac{\partial \log Z}{\partial K_\delta^{(n)}}\right|_{K_\delta^{(n)}=0} = 0$ except for the fixed point, which results in vanishing of the order parameters.

To overcome this issue, we choose half of the spin configurations for a renormalized triangle obtained as a result of n successive RG transformations, where n is sufficiently large. A triangle with Ising spins has $2^3 = 8$ configurations, $\{\uparrow\uparrow\uparrow, \uparrow\uparrow\downarrow, \uparrow\downarrow\uparrow, \downarrow\uparrow\uparrow, \downarrow\downarrow\downarrow, \downarrow\downarrow\uparrow, \downarrow\uparrow\downarrow, \uparrow\downarrow\downarrow\}$,

[2]These limits are not interchangeable, as proved by Rudolph Peierls. It is easy to show that $m = 0$ for a finite-size system under zero magnetic field by using the spin-reversal argument.

where half of them are mostly up and another half are mostly down configurations. The spin configurations we choose are $\{\uparrow\uparrow\uparrow, \uparrow\uparrow\downarrow, \uparrow\downarrow\uparrow, \downarrow\uparrow\uparrow\}$, and for n sufficiently large, only one of these configurations minimize the energy of the system while the probabilities of the other three states go to zero. The eigenvectors of these configurations are:

$$\begin{aligned}
\uparrow\uparrow\uparrow: &\quad \mu^{(n)} = [+1, +1, +1, +1] \,, \\
\uparrow\uparrow\downarrow: &\quad \mu^{(n)} = [+1, +1, -1, -1] \,, \\
\uparrow\downarrow\uparrow: &\quad \mu^{(n)} = [+1, -1, +1, -1] \,, \\
\downarrow\uparrow\uparrow: &\quad \mu^{(n)} = [-1, +1, +1, -1] \,.
\end{aligned}$$

Using one of these eigenvectors such that the corresponding state minimizes the free energy of the renormalized system, one can calculate a finite m and q for each triangle in the pool of triangles, in other words, as a function of the bonds $\{J_{ij}\}$ on a triangle. Ultimately, M and Q are calculated exactly by taking a configurational average over the entire pool.

First we focus on the F bond-percolation case. Its distribution for the entire set of bonds on an AN is given by Eq. 3.3 for $J_{ij} = J > 0$ with probability p and $J_{ij} = 0$ with probability $1 - p$. One may expand the recursion relations in eq. 3.5 into a series in the high-temperature limit, namely for $J_{ij} \ll 1$. For instance, in fig. 3.3, after step (c), the renormalized bond J'_{ij} is equal to the sum of the renormalized bond $\tilde{J}_{ij}$ and the original bond J_{ij} at the edge of the triangle, in other words, $J'_{ij} = J_{ij} + \tilde{J}_{ij}(J_1, J_2, J_3)$. Expanding J'_{ij} into a series in the high temperature limit, under zero magnetic field, the recursion relations for J'_{ij} become

$$\begin{aligned}
J'_{12} &= J_{12} + J_1 J_2 \,, \\
J'_{13} &= J_{13} + J_1 J_3 \,, \\
J'_{23} &= J_{23} + J_2 J_3 \,,
\end{aligned} \tag{3.14}$$

where $J_{ij} = 0$ or $J_{ij} > 0$, and similarly $J_i = 0$ or $J_i > 0$. This result is independent of p, that is, even when $p \ll 1$, in the thermodynamic limit, the flows are in the direction of the strong-coupling limit $J \to \infty$. So, the system is still in the F phase even when the

temperature $T \to \infty$ and $p \to 0$. This analytic argument is also verified with numerical RG flows for the entire range of temperature T and ferromagnetic bond probability p. This type of phenomenon is closely related to the percolation threshold p_c, below which the network is divided into disconnected segments. In AN $p_c = 0$ [50, 59], that is the network stays integrated in large clusters when $p \to 0$, which is related with the infinite-extent order we found on the AN.

In contrast to the F percolation model, the AF percolation model exhibits an infinite-extent SG-like behavior. Its distribution for the entire set of bonds on an AN is given by for $J_{ij} = J < 0$ with probability p, and $J_{ij} = 0$ with probability $1 - p$. In an AF percolation model, depending on whether a loop of bonds in the lattice includes an even or odd number of AF interactions, the loop stays either antiferromagnetic or one of the spins may become frustrated. Thus, it is impossible to derive a simple analytic expression. So to check whether there is a phase transition, we confine ourselves to numerical calculations, again for the entire range of temperature T, and AF bond probability p. We find that for all T and p except for $p = 1$, the model exhibits an SG-like behaviour, so,

$$\langle |J_{ij}| \rangle \to \infty \quad \text{and} \quad \frac{\langle J'_{ij} \rangle}{\sigma_{J'_{ij}}} \to 0\,, \quad \text{for} \quad 0 < p < 1\,. \tag{3.15}$$

The $p = 0$ case is trivial, since there is no system at all, as in the F percolation model. At $p = 1$ all bonds are antiferromagnetic with equal interaction strengths, so $\sigma_{J'_{ij}} = 0$, resulting in a P phase.

In order to check whether there is a P to SG-like phase transition for $0 < p < 1$ on an AN, we introduce another model, which we call the weakened-AF model, where $J_{ij} = J < 0$ with probability p, and $J_{ij} = cJ$ with probability $1 - p$, where $0 < c < 1$. The limits of c are, for $c = 1$, an AN with pure AF bonds of equal strengths, and for $c = 0$, the AF bond percolation model which we covered above. The distribution function of the weakened-AF case for the $\pm J$ model is given by

$$P(J_{ij}) = p\delta(J_{ij} - J) + (1 - p)\delta(J_{ij} - cJ)\,, \quad \text{for} \quad 0 < c < 1\,. \tag{3.16}$$

At very high temperatures, for very high c, such as $c = 0.99$, $\sigma_{J'_{ij}}$ diverges for $p \ll 1$, whereas $\langle J'_{ij} \rangle \to 0$, showing an SG-like behavior everywhere. We conclude that for all percolation models, in the interval $0 < p < 1$, there is no phase transition at all. The AN

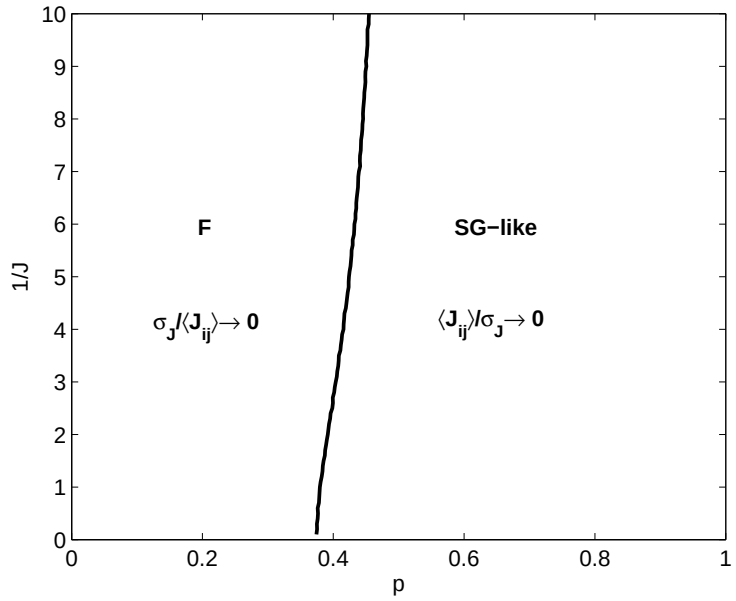

Figure 3.4: Phase diagram of an Ising spin glass on an AN in terms of temperature $1/J$ versus antiferromagnetic bond probability p. At low p values, there is a ferromagnetic phase, whereas at higher p values, there is an SG-like region. The phase boundary is first order and converges to $p = 0.5$ when $T \to \infty$.

topology exhibits an infinite robustness.

The Ising SG model on an AN is even more interesting. Its distribution for the entire set of bonds on an AN is given by eq. 3.2: $J_{ij} = J > 0$ with probability $1-p$, and $J_{ij} = -J$ with probability p. Fig. 3.4 shows the phase diagram of the Ising SG model on an AN. There is a phase transition between the F and SG-like regimes, and the phase boundary converges to $p = 0.5$ for $T \to \infty$. In order to check the order of the phase boundary, and whether the phase on the right hand side of the boundary is in fact an SG phase, we calculate the exact order parameters for each triangle in the pool, that is, as a function of their interaction strengths. A configurational average of the order parameters over the entire pool of triangles gives the average magnetization and SG order parameter of the system as shown in fig. 3.5. There is a discontinuity in the order parameters indicating that there is a first-order phase transition between F and SG-like phases. Furthermore, the magnetization in the SG-like phase converges to zero only when $T \to \infty$ and $p = 0.5$, that is, there are F correlations in the SG-like phase for all temperatures. Additionally,

even if we consider a positive magnetization m near the fixed point, the unrenormalized system chooses a negative magnetization when p is greater than 0.5. This is an intriguing phenomenon which may be unique to scale-free networks: An antiferromagnetic correlation of the few leading spins with a considerable amount of nearest neighbors results in flipping the magnetization, as in the percolation studies on Bàrabasi-Albert networks [60].

The distributions of the order parameters are given in figs. 3.6 and 3.7. We see that the distributions, which are stuck in a narrow interval for high temperatures, extend to intervals $[-1, 1]$ for the magnetization and $[0, 1]$ for the SG order parameter in intermediate temperatures, exhibiting a complicated distribution. For very low temperatures, the spins have either $m = \pm 1$, or $m = 0$ on average, as expected. The evolving distribution of peaks with temperature T and AF bond probability p reveals the highly interesting structure of non-uniform order parameters in pT space. Fig 3.8 shows the nonuniform order parameters versus temperature $T \sim 1/J$ for three different values of AF bond probability p. From these distributions, one can clearly see the ferromagnetism inside the SG-like phase.

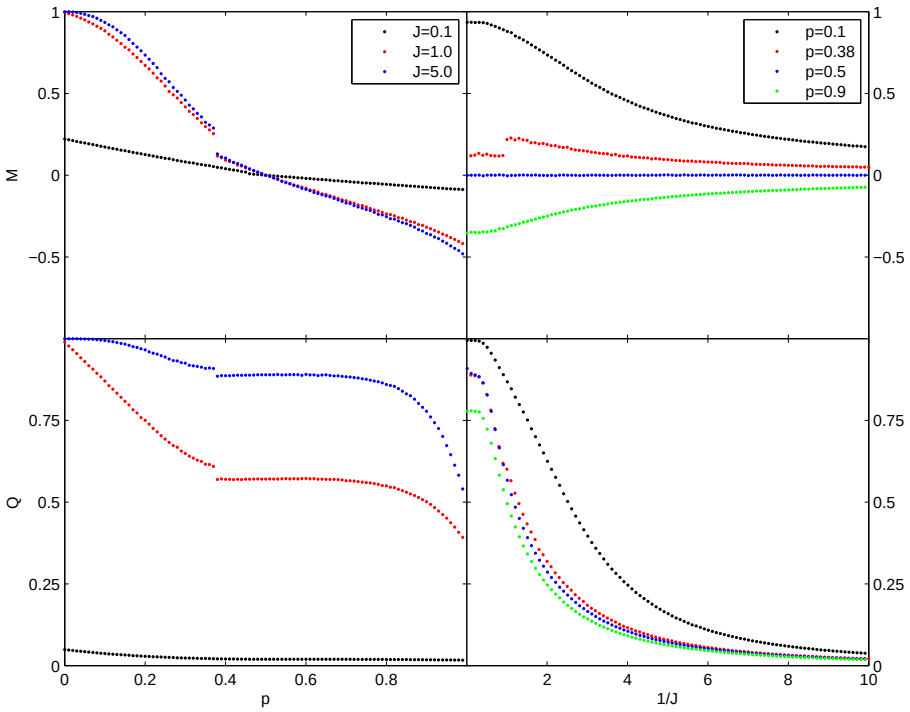

Figure 3.5: The magnetization and spin-glass order parameters versus antiferromagnetic bond probability p (left column) and temperature $1/J$ (right column). The discontinuities in the order parameters indicate that the phase transition is first order.

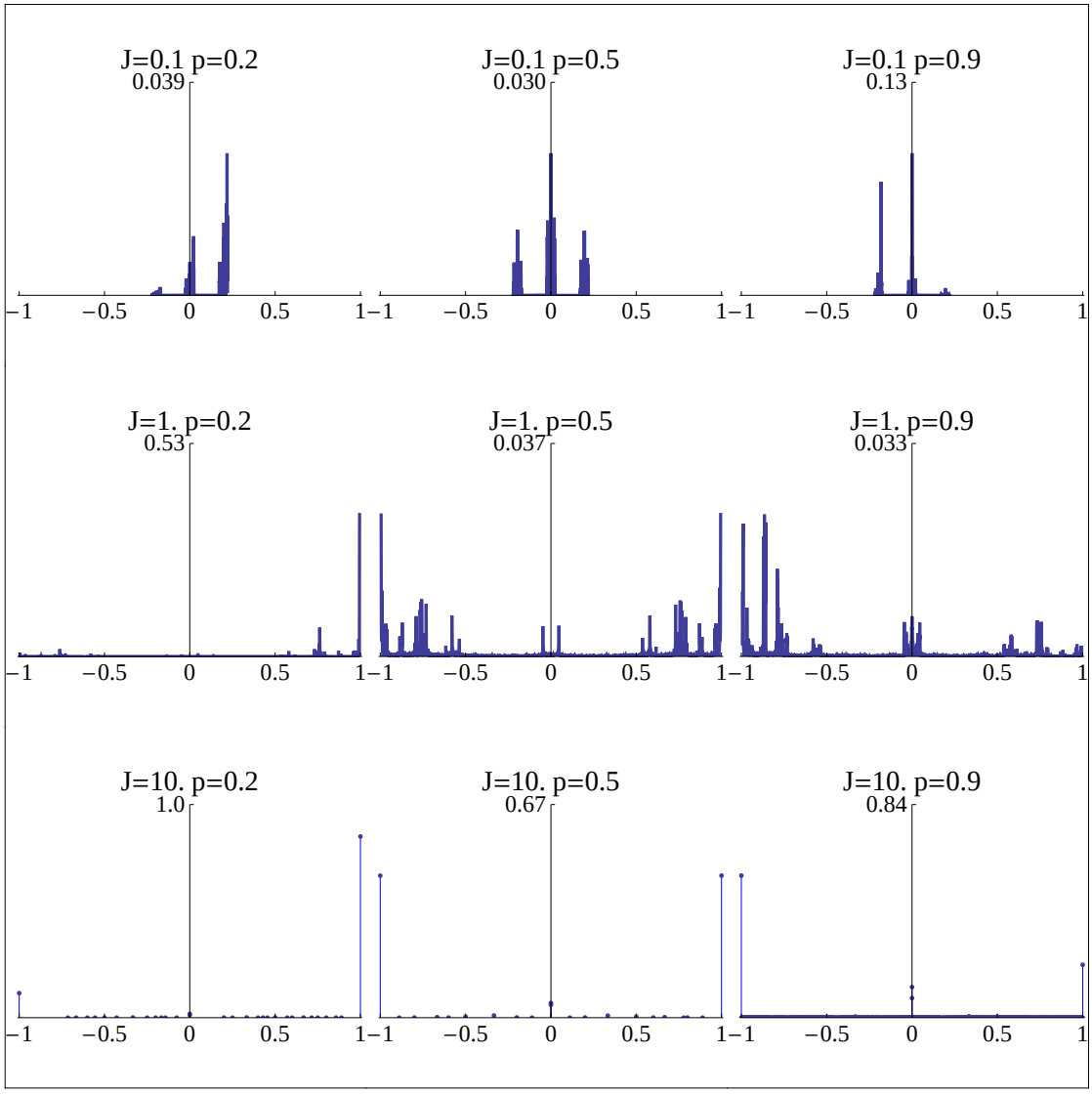

Figure 3.6: The local magnetization distributions in terms of magnetization m versus probability.

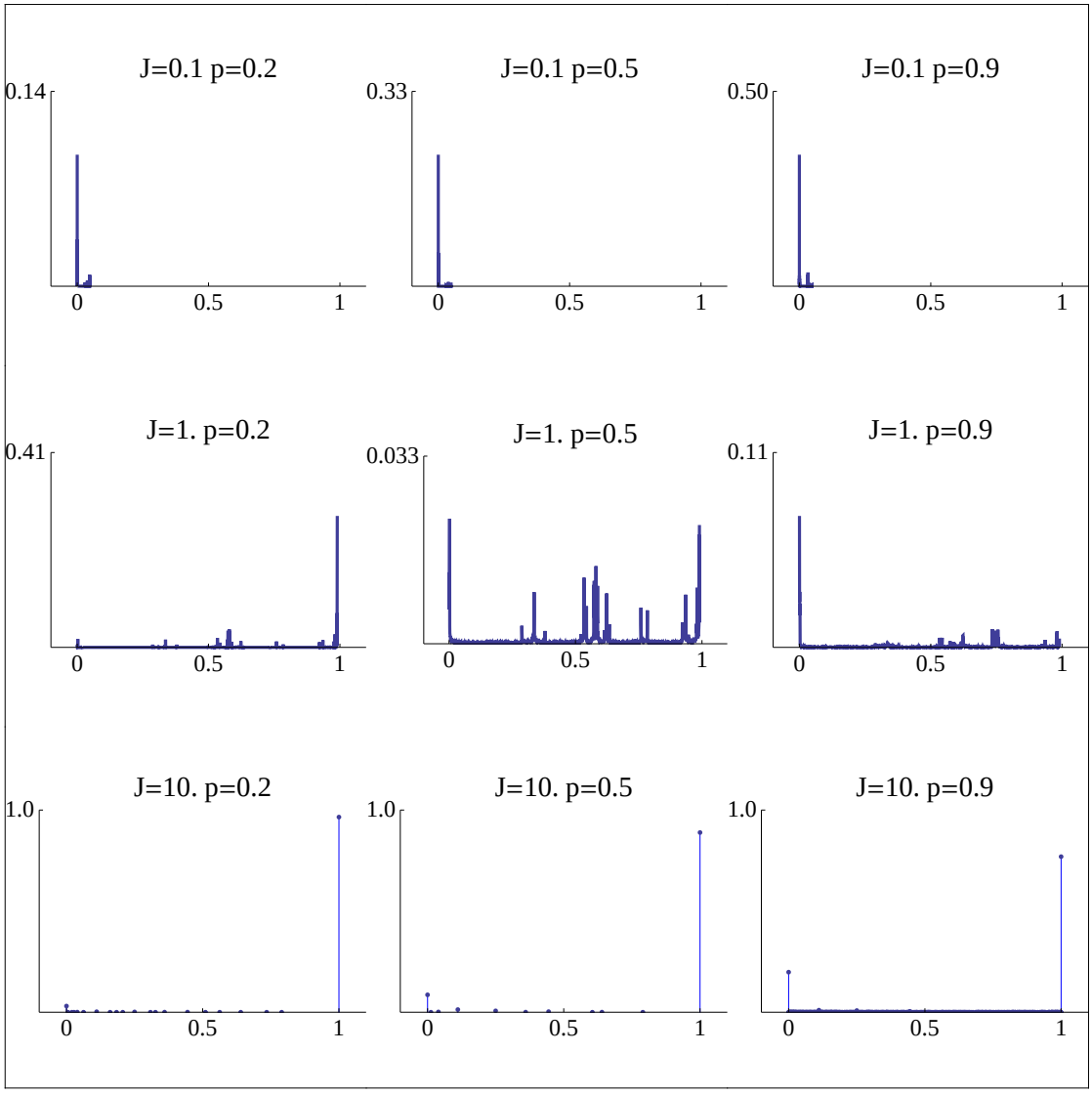

Figure 3.7: The local spin-glass order parameter distributions in terms of q versus probability.

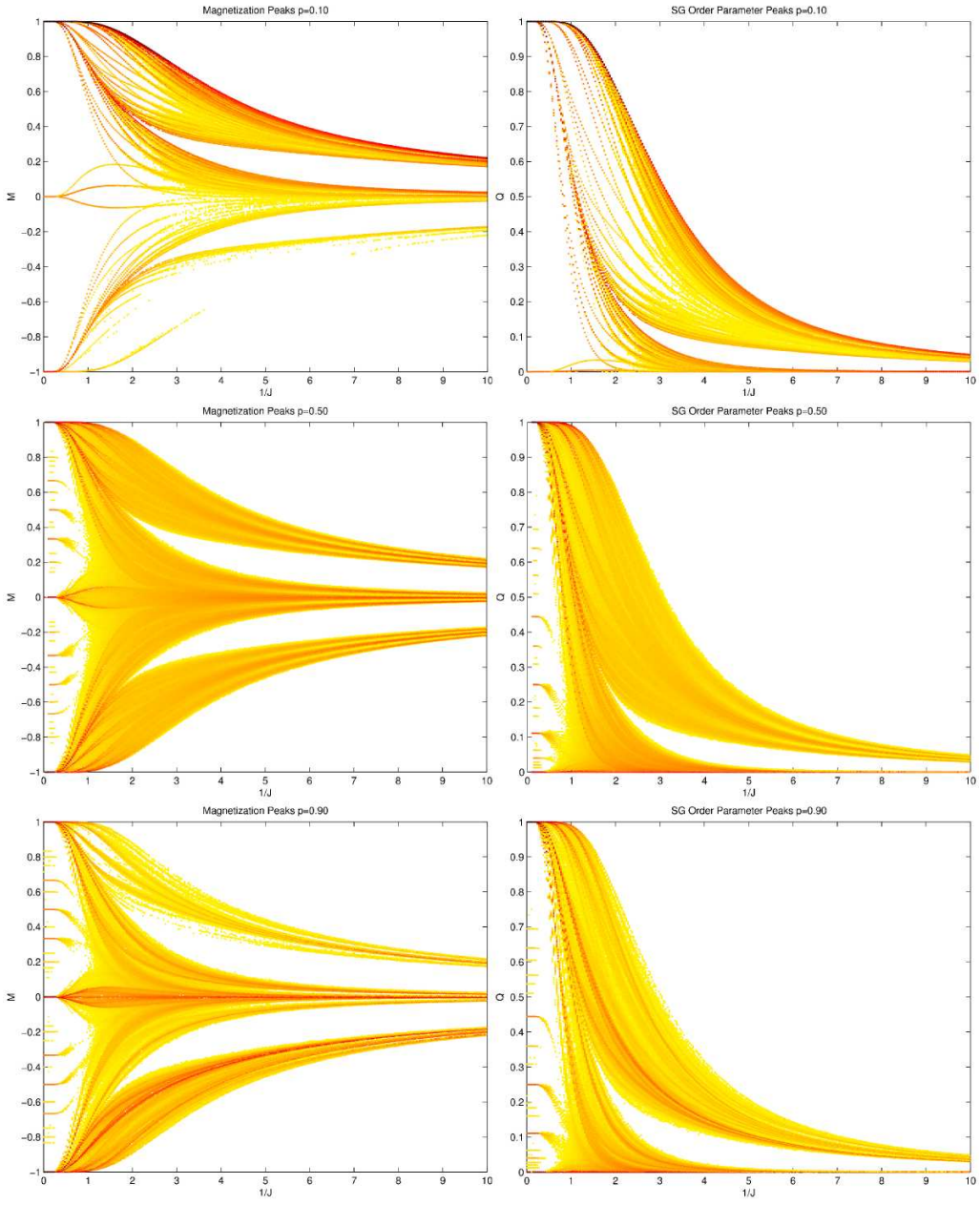

Figure 3.8: The order parameters in terms of m vs. temperature $1/J$ (left column), and in terms of q vs. temperature $1/J$ (right column). From first to last row, $p = 0.2, 0.5, 0.9$, respectively. Colors represent the height of the peaks in Figs. 3.6 and 3.7: the higher a peak, the darker is the corresponding color.

Chapter 4

CONCLUSIONS

The importance of quantum SG models is related to high-T_c superconductivity. In a superconducting material of type II, at $T = 0$, under hole or electron doping depending on the material, there is a phase transition from an AF insulating phase to an SG phase, which has not been explained yet. Our present calculation on quantum Heisenberg nearest-neighbor SG models reveal that there is no phase transition to an SG phase in any dimension. Thus, how an SG phase emerges in a superconducting material is still a challenging question. In addition, the asymmetry in the low temperature phase diagrams indicates a new kind of competition between the ordered phases, not seen in classical models.

Even if a crystal structure is a regular lattice, the question whether an electronic model or a quantum SG model exhibits any SG behavior on a small-world network should also be investigated. Our calculations on a classical SG model produced rich results regarding the SG behavior with ferromagnetic correlations and may motivate the scientific community to the examination of quantum SG models on small-world networks.

Analyzing the AN thermodynamic results shown here, there are important questions to be answered: Do the heights of the histograms in the order-parameter distributions in figs. 3.6 and 3.7 obey a power-law distribution? If so, is the exponent obtained related to any process in real life? Additionally, does the bond probability $p_{m=0}$ where the magnetization goes to zero, e.g. $p_{m=0} = 0.5$ in fig. 3.5, depend on the exponent of the power-law degree distribution? Depending on the height of the tail of $P(k)$ when k is large, the value $p_{m=0} = 0.5$ may shift either towards the $p = 1$ or $p = 0$ directions.

For future work, we are interested in both whether the non-uniform order parameters exhibit a power-law behavior, and the relation between the order parameters and power-law behaviours of the degree distribution in small-world networks.

BIBLIOGRAPHY

[1] C.N. Kaplan and A.N. Berker, Phys. Rev. Lett. **100**, 027204 (2008).

[2] C.N. Kaplan, M. Hinczewski, and A.N. Berker, preprint (2008).

[3] H.E. Stanley, *Inroduction to Phase Transitions and Critical Phenomena* (Oxford University Press, 1987).

[4] J.M. Yeomans, *Statistical Mechanics of Phase Transitions* (Oxford University Press, 1992).

[5] J.P. Sethna, *Statistical Mechanics: Entropy, Order Parameters, and Complexity* (Oxford University Press, 2006).

[6] L.P. Kadanoff, Physica **2**, 263 (1966).

[7] K.G. Wilson, Phys. Rev. B **4**, 3184 (1971).

[8] D.R. Nelson and M.E. Fisher, Ann. Phys. **91**, 226 (1975).

[9] H. Nishimori, *Statistical Physics of Spin Glasses and Information Processing, An Introduction* (Oxford University Press, 2001).

[10] G.S. Rushbrooke and P.J. Wood, Mol. Phys. **6**, 409 (1963).

[11] J. Oitmaa and W. Zheng, J. Phys.: Condens. Matter **16**, 8653 (2004).

[12] A. Falicov and A.N. Berker, Phys. Rev. B **51**, 12458 (1995).

[13] M. Hinczewski and A.N. Berker, Eur. Phys. J. B **48**, 1 (2005).

[14] A.N. Berker and S. Ostlund, J. Phys. C **12**, 4961 (1979).

[15] R.B. Griffiths and M. Kaufman, Phys. Rev. B **26**, 5022R (1982).

[16] M. Kaufman and R.B. Griffiths, Phys. Rev. B **30**, 244 (1984).

[17] A. Erbaş, A. Tuncer, B. Yücesoy, and A.N. Berker, Phys. Rev. E **72**, 026129 (2005).

[18] M. Hinczewski and A.N. Berker, Phys. Rev. E **73**, 066126 (2006).

[19] M. Hinczewski, Phys. Rev E **75**, 061104 (2007).

[20] Z. Zhang, L. Rong, and S. Zhou, Physica A **377**, 329 (2007).

[21] Z. Zhang, S. Zhou, and T. Zou, Eur. Phys. J. B **56**, 259 (2007).

[22] H.D. Rozenfeld and D. ben-Avraham, Phys. Rev. E **75**, 061102 (2007).

[23] H.D. Rozenfeld, S. Havlin, and D. ben-Avraham, New J. Phys. **9**, 175 (2007).

[24] E. Khajeh, S.N. Dorogovtsev, and J.F.F. Mendes, Phys. Rev. E **75**, 041112 (2007).

[25] M. Suzuki and H. Takano, Phys. Lett. A **69**, 426 (1979).

[26] H. Takano and M. Suzuki, J. Stat. Phys. **26**, 635 (1981).

[27] P. Tomczak, Phys. Rev. B **53**, R500 (1996).

[28] P. Tomczak and J. Richter, Phys. Rev. B **54**, 9004 (1996).

[29] P. Tomczak and J. Richter, J. Phys. A **36**, 5399 (2003).

[30] M. Hinczewski and A.N. Berker, Eur. Phys. J. B **51**, 461 (2006).

[31] M. Hinczewski and A.N. Berker, Phys. Rev. B, in press (2008).

[32] C.N. Kaplan, A.N. Berker, and M. Hinczewski, preprint (2007).

[33] O.S. Sarıyer, A.N. Berker, and M. Hinczewski, Phys. Rev. B **77**, 134413 (2008).

[34] A. Falicov, A.N. Berker, and S.R. McKay, Phys. Rev. B **51**, 8266 (1995).

[35] G. Migliorini and A.N. Berker, Phys. Rev. B **57**, 426 (1998).

[36] H. Nishimori and S.J. Miyake, Prog. Theor. Phys. **73**, 18 (1985).

[37] S. Ostlund and A.N. Berker, Phys. Rev. B **21**, 5410 (1980).

[38] D. Sherrington and S. Kirkpatrick, Phys. Rev. Lett. **32**, 1792 (1975).

[39] A.J. Bray and M.A. Moore, J. Phys. C **13**, L655 (1980).

[40] B. Yücesoy and A.N. Berker, Phys. Rev. B **76**, 014417 (2007).

[41] D.J. Watts and S. H. Strogatz, Nature (London) **393**, 440 (1998).

[42] T. Zhou, G. Yan, B.-H. Wang, Phys. Rev. E **71**, 046141 (2005).

[43] M. Faloutsos, P.Flaoutsos, and C. Faloutsos, Comput. Commun. Rev. **29**, 251 (1999).

[44] R. Pastor-Satorras, A. Vàzquez, and A. Vespignani, Phys. Rev. Lett. **87**, 258701 (2001).

[45] G. Caldarell, R. Marchetti, and L. Pietronero, Europhys. Lett. **52**, 386 (2000).

[46] A.G. Phadke, J.S. Thorp, *Computer Relaying for Power Systems* (Wiley, New York, 1988).

[47] A.-L. Barabàsi and R. Albert, Science **286**, 509 (1999).

[48] A.-L. Barabàsi, R. Albert, and H. Jeong, Physica A **272**, 173 (1999).

[49] M.E.J. Newman and D.J. Watts, Phys. Lett. A **263**, 341 (1999).

[50] J.S. Andrade, H.J. Hermann, R.F.S. Andrade, and L.R. da Silva, Phys. Rev. Lett. **94**, 018702 (2005).

[51] Z.Zhang, L. Chen, S. Zhou, L. Fang, J. Guan, and T. Zou, Phys. Rev. E **77**, 017102 (2008).

[52] Z. Zhang and S. Zhou, cond-mat/0609270.

[53] Z. Zhang, L. Rong, S. Zhou, Phys. Rev. E **74**, 046105 (2006).

[54] G. Oron and H.J. Hermann, J. Phys. A:Math. Gen. **33**, 1417 (2000).

[55] A.M. Souza and H. Hermann, Phys. Rev. B **75**, 054412 (2007).

[56] R. Albert, H. Jeong, A.-L. Barabàsi, Nature (London) **406**, 378 (2000).

[57] F. D. Nobre, Phys. Rev. E **64**, 046108 (2001).

[58] M. Ohzeki, H. Nishimori, and A.N. Berker, Phys. Rev. E **77**, 061116 (2008).

[59] R. Cohen, K. Erez, D.B. Avraham, and S. Havlin, Phys. Rev. Lett. **85**, 21 (2000).

[60] A. Aleksiejuk, J.A. Holyst, and D. Stauffer, Physica A **310**, 260-266 (2002).

VITA

CİHAN NADİR KAPLAN was born in Karadeniz Ereğli, Turkey, on December 6, 1982. He graduated from the German High School in 2001. He got his Bachelor of Science in Physics Engineering from Istanbul Technical University (ITU) in 2006. In August 2006, he was accepted to M.S. program in physics with full scholarship in Koç University. In high school and during his undergraduate studies, he wrote articles about computer hardware and software in magazines such as PC Magazine, Tom's Hardware, etc., and co-founded PC Labs, which is currently the leading computer hardware software news and review web site in Turkey. He also held singing activities in well-known choirs such as the German High School Choir and the European Choir, and a recently founded room choir called Korİst. He gave various concerts both in Turkey and abroad. He wrote three research articles about high-T_c superconductivity, quantum spin-glasses and small-world networks to date, one of them published in Physical Review Letters and two of them about to be submitted. He gave one invited talk in 2006, at the Max-Planck Institute (Dresden, Germany), and two contributed talks at the 98th. Statistical Mechanics Meeting (New Brunswick, NJ, U.S.A.) and at the APS March Meeting 2008 (New Orleans, LA, U.S.A.). He will continue his doctoral studies in Brandeis University, U.S., where he will focus on the physics of biological systems. At the present time, he has an ongoing nanotechnology project about the dynamics of water in carbon nanotubes where he collaborates with Prof. Roland R. Netz and his research group at the Technical University of Munich (TUM).